34th Space Symposium, Technical Track, Colorado Springs, Colorado, United States of America
Presented on April 16, 2018

Enhancing Finite Element Analysis with Digital Image Correlation Point Cloud Test Data

Matt Sanders, PE
Stress Engineering Services, Inc., Matt.Sanders@Stress.com

Vishal Nayyar, PhD
Stress Engineering Services, Inc., Vishal.Nayyar@Stress.com

Patrick Whalen, PE
Stress Engineering Services, Inc., Patrick.Whalen@Stress.com

Taylor Yeary
Stress Engineering Services, Inc., Taylor.Yeary@Stress.com

ABSTRACT

The ability to gain insight into how launch vehicles perform through analysis and testing has always been important, and with a new shift towards rocket reusability in trying to reduce launch costs, it is even more critical. Balancing the highly dynamic and extreme loads during take-off with the complex and intricate weight-reducing vehicle structural designs has challenged engineers evaluating new concepts for performance. When these complex structures are pushed to be increasingly reusable, it is even more important to understand how loads are distributed through a structure in order to predict success, not only on the first launch, but on subsequent launches as well. Finite Element Analysis (FEA) with empirical testing, and their correlation at discrete points, have traditionally represented major tools in this area; however, linking the two can be a challenge. New tools such as Digital Image Correlation (DIC) can be coupled with FEA to aid in analyzing and predicting the response of materials and structures under load, which is vital for aerospace applications. In taking advantage of new advances in DIC, proper testing methods, and an in-depth understanding of FEA; a better link can be established between analysis and testing. Various assumptions used in FEA modeling can now be more accurately validated using a point cloud database of real-world test data for the actual part being analyzed, instead of discrete points. This paper highlights several experiences in using DIC and photogrammetry tools to gain understanding in this area. Three case studies are presented: an aluminum 6061 uniaxial tensile test to failure, a carbon-fiber tube with a hole in bending compression, and an additive-manufactured Alloy 718 nozzle. For each case study, approaches and results are discussed for utilizing DIC and FEA together to improve the correlation between analysis and full-scale testing.

NOMENCLATURE

AM	=	Additive Manufactured	FOV	=	Field of View
ASME	=	American Society of Mechanical Engineers	HIP	=	Hot Isostatic Pressing
ASTM	=	American Society of Testing and Materials	MTRs	=	Material Test Reports
CAD	=	Computer Aided Design	PBLS	=	Powder Bed Laser Sintering
DIC	=	Digital Image Correlation	RWS	=	Real World System
FEA	=	Finite Element Analysis	SCF	=	Stress Concentration Factor
FEM	=	Finite Element Model	ue	=	Microstrain [in/in x $1x10^6$]
FOS	=	Factor of Safety	V & V	=	Verification and Validation

INTRODUCTION

Lifting humans and payloads into Earth orbit and beyond is extremely difficult and requires complex high-performance equipment. Today, powerful design tools are available that use computer programs to generate optimized design solutions. Combining these computer tools with the advancements in materials, CNC machining,

and additive manufacturing, results in components that are significantly stronger, lighter, and more complex than designs produced using conventional design and manufacturing methods.

With this complexity, engineers are faced with the difficult task of trying to evaluate designs for performance. Advances in computer software and hardware technologies have allowed aerospace designs as well as advanced materials to be analyzed with more intricate Finite Element Models (FEM) than ever before. Because every conceived design cannot be full-scale tested for performance, engineers turn to FEA to help evaluate new designs and concepts. Computer modeling and analysis, however, does have limitations. The American Society of Mechanical Engineers has stated, "Scientists and engineers [should] be aware that the computational models they develop and use are approximations of reality and that these models are subject to the limitations of available data, physical theory, mathematical representations, and numerical solutions."[1] A paper by NASA commented that, "Young engineers are becoming increasingly efficient in building complex 3D models of complicated aerospace components. However, the current trends demonstrate blind acceptance of the results of the finite element analysis."[2] Therefore it is highly important to validate FEA with empirical test data. Validation is the process of determining how accurately an FEM represents its real-world counterpart.[3]

Correlating test data with the FEA can be a difficult task, and high costs of full-scale state-of-the art testing can limit the use of extensive test programs to cover all possibilities or design iterations. Strain gages have traditionally been used to measure the response of structures at discrete locations under load to compare the outputs with the corresponding FEM. This method has worked well; however, some limitations exist.

3D Digital Image Correlation (DIC), through its full field of data, is increasingly being considered as a viable tool for helping bridge the gap between FEA and empirical testing. In one study, DIC and FEA techniques were used together to gain a deeper understanding of tensile and shear stress failures in stainless steel and titanium brazed with aluminum 1100 for use in aerospace structures.[4] DIC test data and FEA have also been used to develop progressive damage analysis tools for predicting the strength of composite bonded joints.[5] The technique has been used in a wide variety of applications[6], from aerospace applications such as evaluating the buckling of high-performance thin wall launch vehicle shell structures[7] and thermoplastic composite panels[8], to medical applications such as evaluating human tissue[9] and teeth[10]. One particular study[11] used DIC test data to fine-tune an FEA model to be able to predict buckling loads in large-scale launch vehicle structures to within 2%.

A recent study used FEA, supported with DIC test data, to optimize the design of a force balance for increased fatigue performance. Multidimensional force transducers, commonly referred to as force balances, are devices instrumented with strain gages that are used to measure the various components of aerodynamic loads in aeronautics wind-tunnel testing. The authors of the study found that the results of their FEA provided good global three-dimensional contour plots of the stress and strain field distributions in the force balances under certain loads. However, the models needed to be validated and properly configured using DIC test data.[12]

The approach of this paper is to describe a few example case studies of situations where FEA did not exactly correlate with empirical test results and to offer commentary on why and what steps can be taken to refine both the FEA and testing methods. The case studies highlighted were chosen to demonstrate increasing levels of complexity. The overall goal is to demonstrate how FEA and DIC can be employed together to gain a better understanding of the responses of materials and structures under loading conditions.

Digital Image Correlation

For each case study, 3D DIC was used for data acquisition during the physical testing. A DIC system is an optical-based system for measuring surface strain and displacement. A stochastic speckle (or dot) pattern is first applied to the surface to be measured. The surface is then photographed under various loading conditions. The DIC system software recognizes and tracks the surface pattern, and is able to measure minute changes in the pattern. The software algorithm creates facets of a fixed number of pixels, identified by the unique pattern in each facet, as shown in Exhibit 1**.** When the surface is subjected to load or otherwise deforms or displaces, the facets deform and/or shift.

These deformations are measured by the software and used to calculate the corresponding surface strains and displacements.

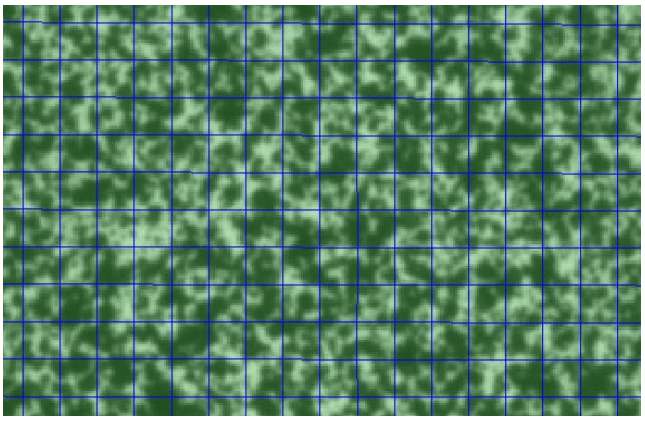

Exhibit 1: Speckled surface showing a representation of the DIC Facet Field.

Unlike other strain and displacement measurement devices (such as strain gages), DIC provides full field strain and displacement, providing measurements at any locations that can be sufficiently photographed. DIC also requires no contact between the measuring device (the camera) and surface. The only requirement is that the surface must be prepared with a speckle pattern. This can be performed using a number of methods, including ordinary spray paint.

DIC systems can employ one camera for 2D measurement of in-plane displacements and strains, or a stereo camera pair to measure in 3D and capture out-of-plane displacements. The cameras are calibrated together to allow accurate 3D distance and deformation measurements and account for any lens distortion. The 3D DIC system combines the stereoscopic technique of the two cameras together and the DIC system software.[13,14] This allows for strains and displacements to be measured in three dimensions. Stress Engineering Services' DIC system, used for measurements in the case studies provided here, used a stereo camera pair as shown in Exhibit 2. The 3D-DIC system used for these case studies was the commercially available GOM Aramis Version 6.3.1.

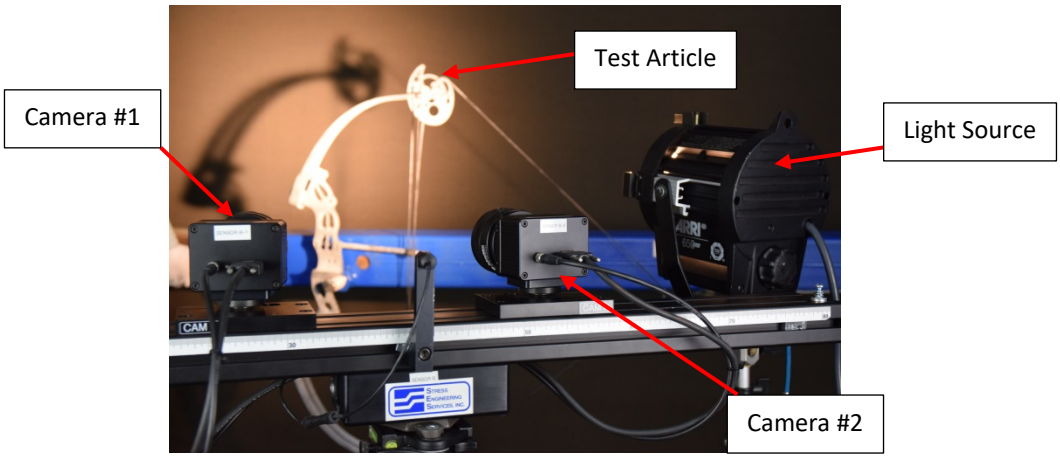

Exhibit 2: DIC Camera System.

For each of the case studies, a speckle pattern was applied to the sample to be tested using spray paint. After allowing the speckle pattern to dry, each specimen was tested. The surface displacements were recorded using the DIC system, and surface strains calculated. Exhibit 3 shows the standard set-up: two cameras were used to take images of the specimen's region of interest, which was prepared with the speckle pattern. The spacing of the

cameras, the lenses used, and the distance between the sample and the cameras were adjusted per the software system's specifications to achieve the desired field of view.[15] The field of view of the two cameras was adjusted so that the speckled region of the specimen was always visible and maximized in the field of view as the test was performed.

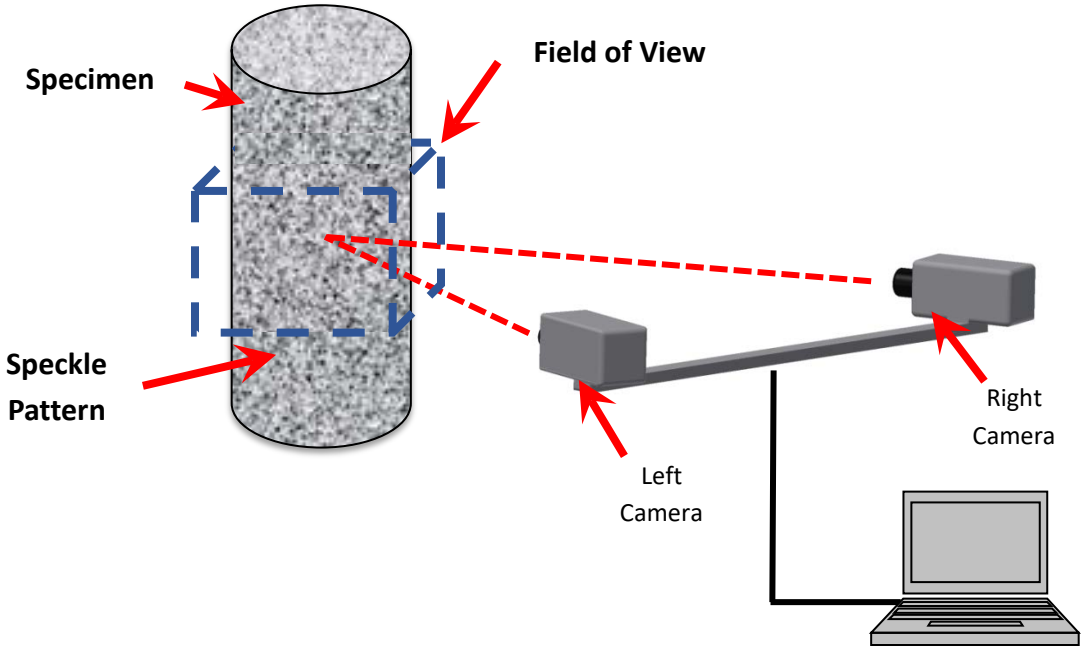

Exhibit 3: Schematic of standard 3D-DIC set-up used for tests.

CASE STUDIES

Descriptions and discussions for three case studies are provided in the following sections. The cases were chosen to demonstrate uses of FEA and DIC on simple to more complex geometries and materials, as well as investigate factors that can cause difficulty in both FEA and testing, and how these two can be used together to improve analysis methodology.

1. Uniaxial tensile test of an isotropic material with well understood properties (aluminum 6061).
2. Four-point bend test of a tube with an added defect made of carbon-fiber composite.
3. Compression test of a complex Alloy 718 nozzle formed using additive manufacturing (AM).

Case Study 1: Aluminum Tensile Coupon

The first case study compared FEA and testing results of an aluminum 6061 flat bar tensile coupon. Exhibit 4 shows the test model used to simulate the uniaxial tension test performed. The Abaqus general-purpose FE software (version 6.14-1) was used for meshing and performing the analyses.[16] Nearly 64,000 3D solid elements (C3D8R) were used to create the mesh (Exhibit 5). The force was applied on one end of the coupon, based on the force used during the uniaxial tension test. The load was applied as a static load. Large deformation theory was used in the analysis.

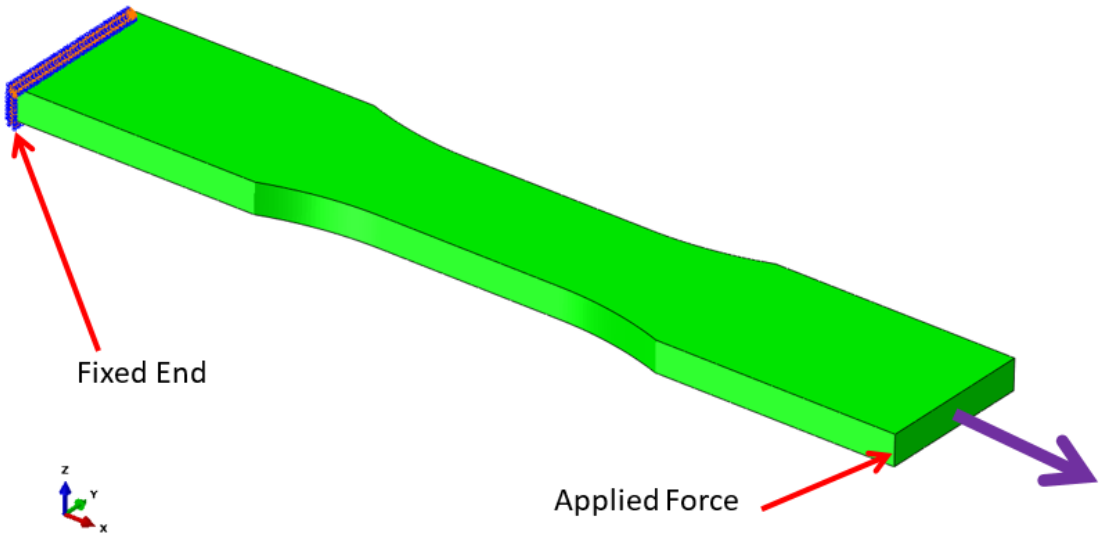

Exhibit 4: Loads and boundary conditions applied in the Coupon Model

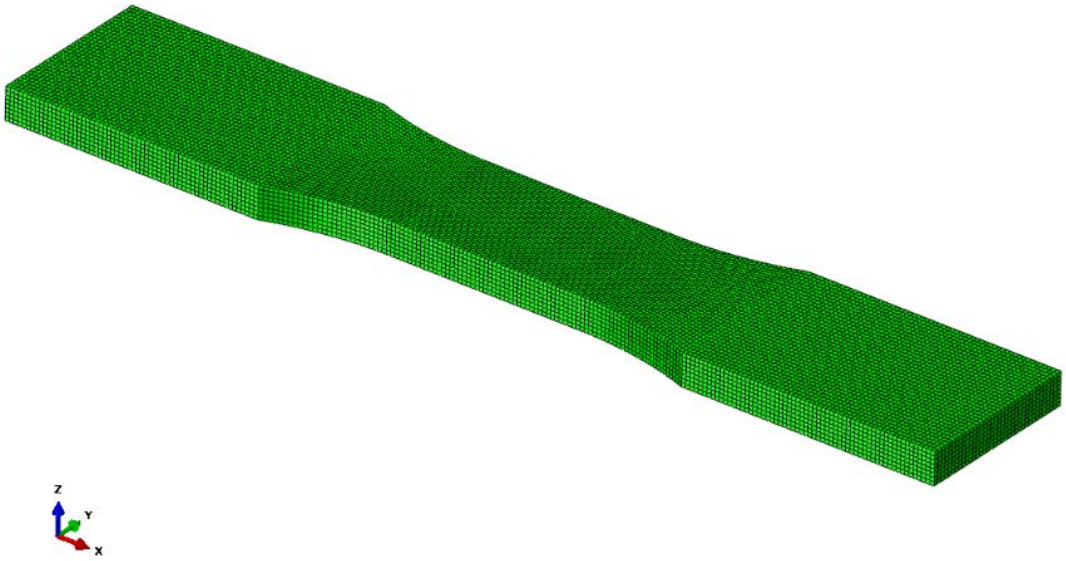

Exhibit 5: Finite Element Model mesh

For comparison to the Finite Element Model (FEM), an ASTM A370 uniaxial tensile test was conducted on a 1.5 inch X 0.375 inch flat bar aluminum 6061 coupon. Exhibit 6 shows the overall test set-up and Exhibit 7 shows the tensile test coupon. The speckle pattern can be seen in Exhibit 7 as well as the extensometer clip gage that is typically used to measure the elongation during this type of test.

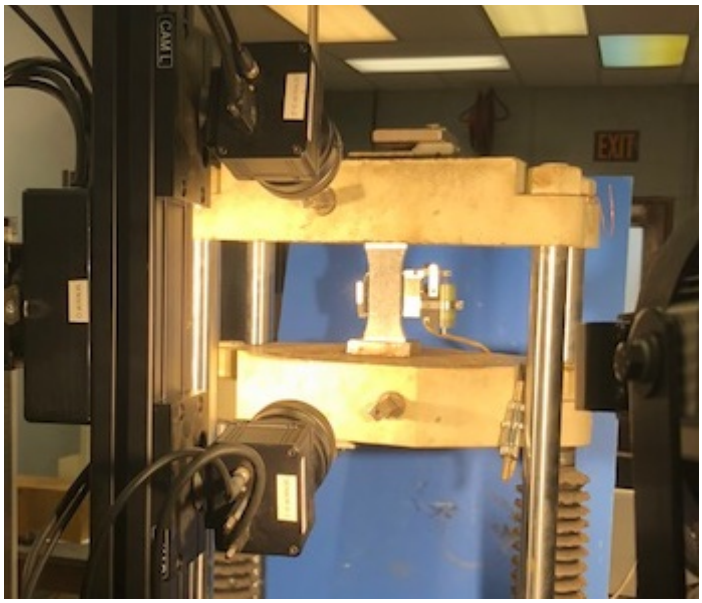

Exhibit 6. DIC measurement performed on an aluminum coupon during tensile testing.

Exhibit 7. Aluminum coupon installed in tensile testing machine with 2 inch clip gage attached and surface speckled pattern for DIC.

Exhibit 8 shows a comparison of the axial strain contour plots obtained via the DIC and FEA. A virtual cross-section line was drawn down the center of the test coupon and the axial strains were plotted along that line. FEA and DIC generated strains along that cross section at an applied tension load of 24,700 lbf, shortly after yield of the sample, are shown in Exhibit 9. This comparison illustrates one of the advantages of using DIC to compare to FEA. Traditional empirical testing with strain gages or extensometers would not enable generating this type of data. The

FEA strains are consistently lower than the DIC measured strains across the cross-section, indicating that the FEM is not completely accurately modeling the post-yield behavior of the aluminum sample.

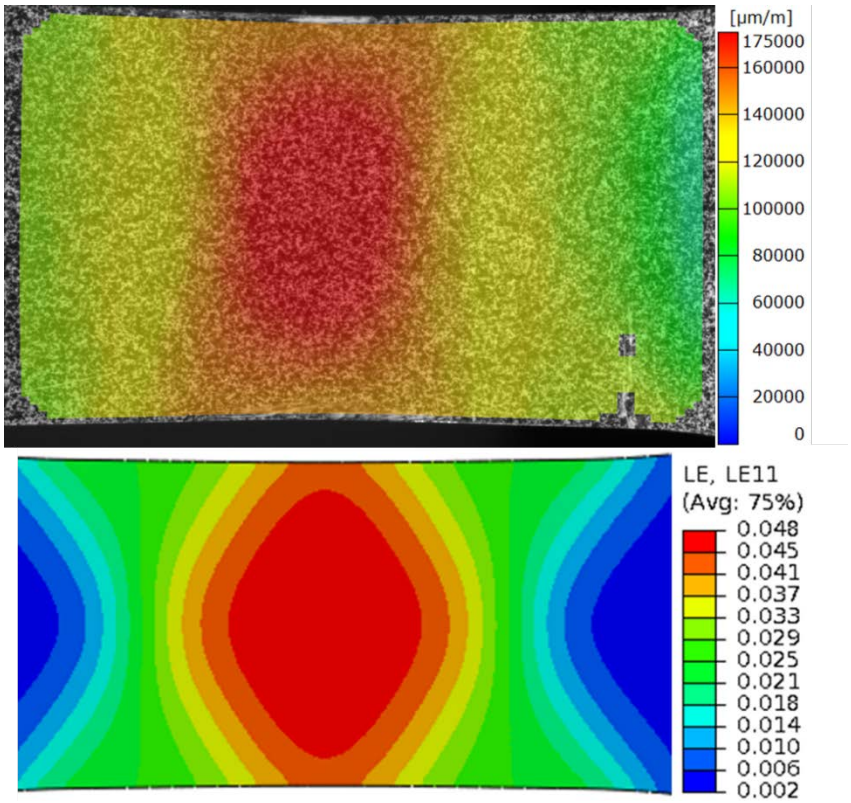

Exhibit 8: Comparison of strain fields obtained via DIC (top) and FEA (bottom).

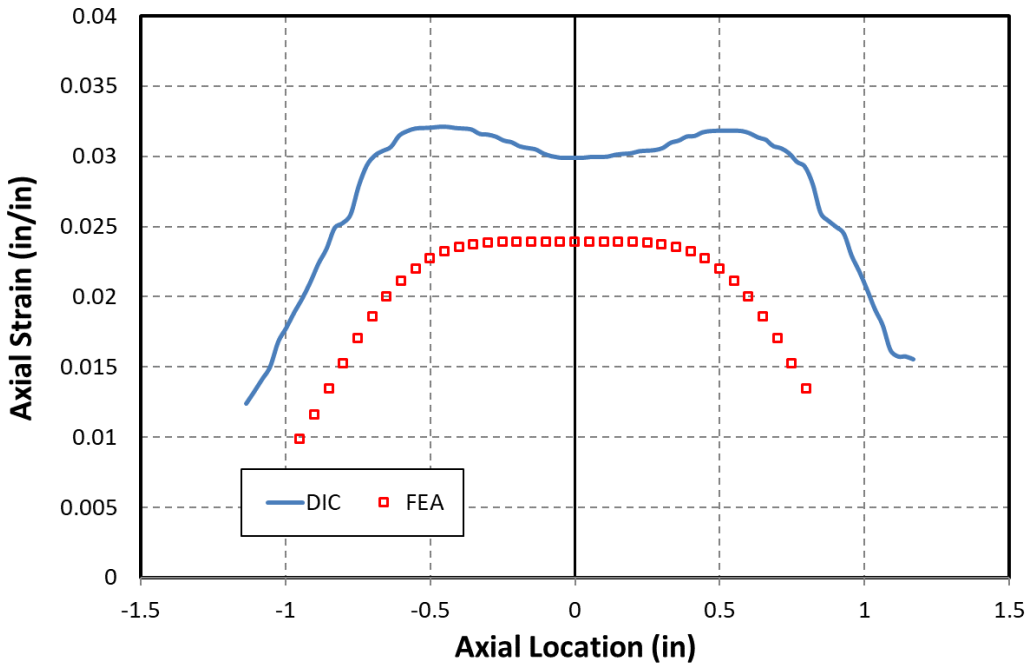

Exhibit 9: Axial strain comparison along the center of the coupon (24,700 lbf applid load).

Exhibit 10 shows a stress/strain curve generated via tensile testing of the aluminum 6061 coupon. The dashed line represents the displacement measured with a clip gage with an initial gage length of 2 inches. After yielding of the material occurred, the test lab removed the clip gage so that it would not exceed its maximum displacement, as is standard practice for this type of test. The solid line in Exhibit 10 represents the displacement measured by the DIC system also over an initial gage length of 2 inches, as shown in Exhibit 6 and Exhibit 7. The DIC system was able to record displacement and strain all the way to failure of the test coupon.

Using the DIC data, the behavior of the 6061 Aluminum in the plastic region (post-yield) and at failure can be much better defined in an FEM than by using the load and clip gage data alone. Using this data, the FEM properties could be refined to more closely match the real world conditions, and correct for the error seen in Exhibit 9.

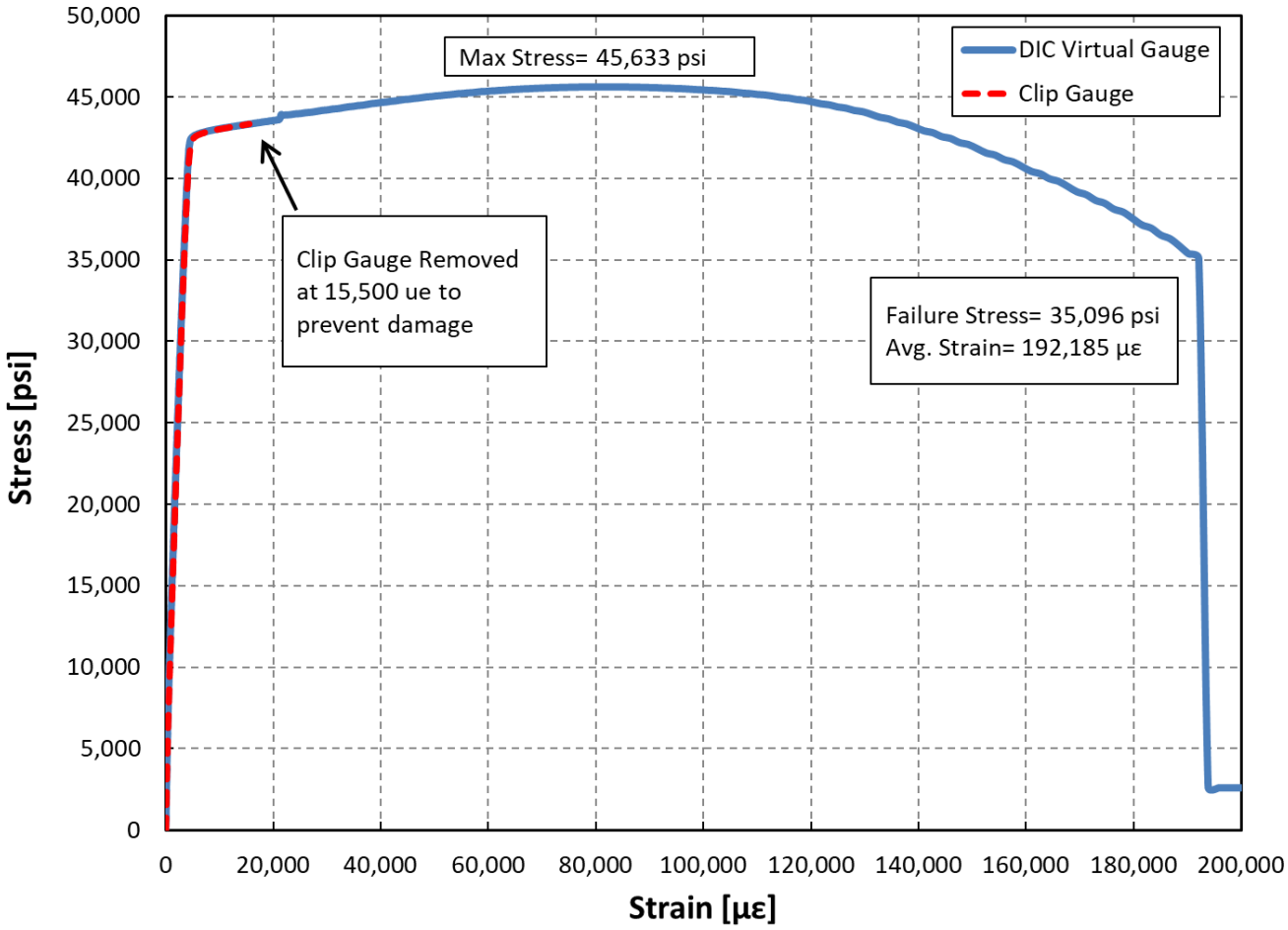

Exhibit 10: Aluminum coupon tensile testing stress/strain curve.

Case Study 2: Carbon Fiber Composite Tube with Stress Concentration in Four-Point Bending

To investigate the correlation between FEA and DIC on anisotropic materials, the Abaqus finite element software was used for meshing and performing the analysis of a bending test of a composite tube with a hole installed to create a stress concentration.

Exhibit 11 shows the model of the composite tube used to simulate the bending test performed. A quarter symmetry model was used in the analysis. The material is carbon fiber composite with an OD of 1.008 inches and wall thickness of 0.035 inch. The material parameters used for modeling the composite tube are listed in Table 1.

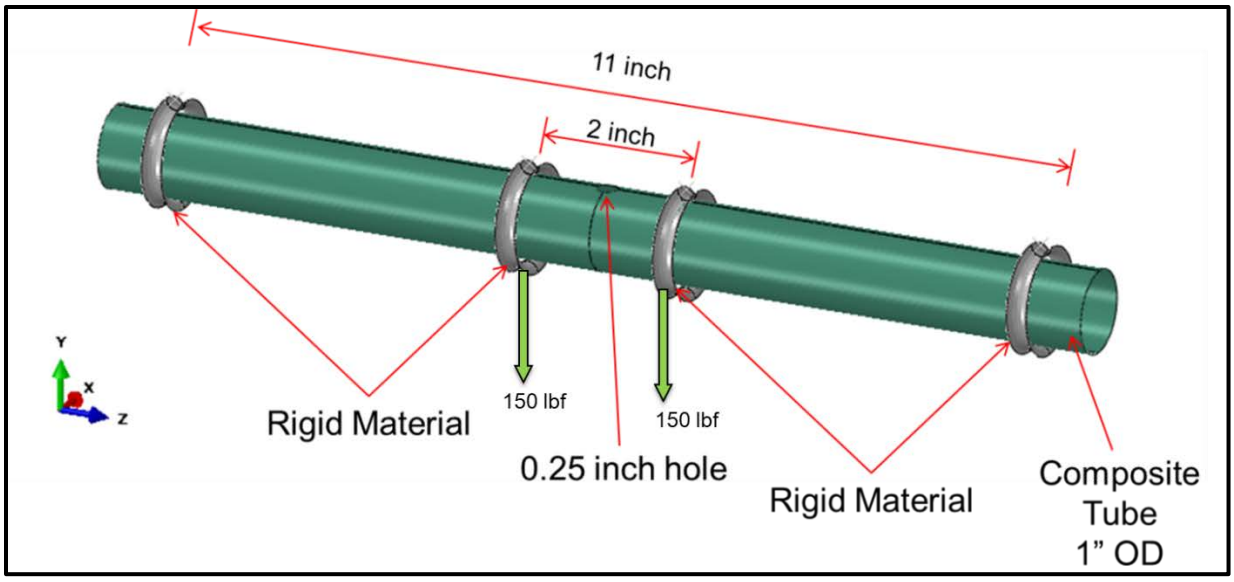

Exhibit 11: Finite element model for Composite Tube.

The tube was modeled as a five-ply composite material with fiber orientation of each layer as shown in Table 2 and Exhibit 12. The supports were modeled as rigid material. Both the tube and supports were modeled as shells using S4R type elements in Abaqus. Nearly 25,000 elements were used in the model with element size of approximately 0.02" x 0.02". Exhibit 13 shows the mesh used for the composite tube analysis. A total static load of 300 lbf was applied on the tube, equally distributed between the two center indenters. Large deformation theory was used in the analysis. The outer supports were kept fixed and a surface-to-surface contact was modeled between the supports and tube with friction coefficient of 0.1.

Table 1: Material Properties for Composite Tube.

Parameter	Value
Tensile Modulus along x-direction, E_x (psi)	21,600,000
Tensile Modulus along y-direction, E_y (psi)	12,800,000
Tensile Modulus along z-direction, E_z (psi)	12,800,000
Poisson's ratio along xy-direction, ν_{xy}	0.342
Poisson's ratio along xz-direction, ν_{xz}	0.342
Poisson's ratio along yz-direction, ν_{yz}	0.35
Shear Modulus, G_{xy} (psi)	780,000
Shear Modulus, G_{xz} (psi)	780,000
Shear Modulus, G_{yz} (psi)	413,720

Table 2: Fiber orientation for composite material.

Ply Number	Fiber Orientation
Ply 1 (ID)	0°
Ply 2	0°
Ply 3	90°
Ply 4	90°
Ply 5 (OD)	0°/90° alternating

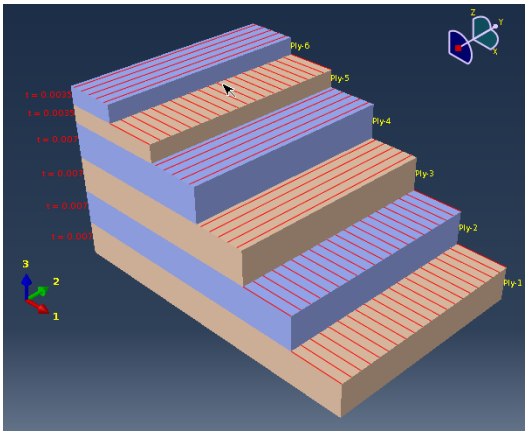

Exhibit 12: Composite Tube FEM fiber orientation**.**

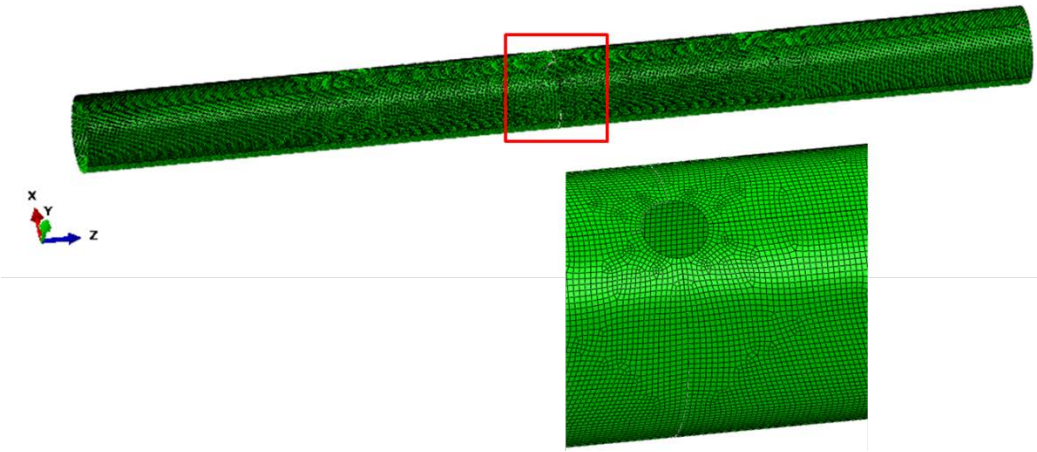

Exhibit 13: Finite Element Model mesh for composite tube.

An actual carbon tube was then prepared with a DIC speckle pattern and load tested with a four-point bending method as shown in Exhibit 14. Unlike the FEM, the outer ply of the physical carbon tube was made up of 0° and 90° fibers woven together, instead of the half-thickness layers shown in Exhibit 12. This difference was not captured in the FEM due to the limitations of the FEA software. To match the analysis, the 0.25-inch hole was placed in the bending plane on the compression side of the bend (0° Orientation). This area was monitored with the DIC system as a bending moment was applied incrementally via a screw jack at the center supports. The applied load was determined by an NIST traceable load cell. The tube was loaded incrementally until failure of the composite tube occurred. Throughout testing, fiber cracking sounds were heard at various increments without significant loss of global tube stiffness. At an applied load of 300 lbf, soon after one set of DIC images was captured, extreme local fiber buckling occurred adjacent to the hole location, resulting in a rapid loss of compressive strength of the sample. Various load points were then chosen for comparison between the DIC results and FEA model.

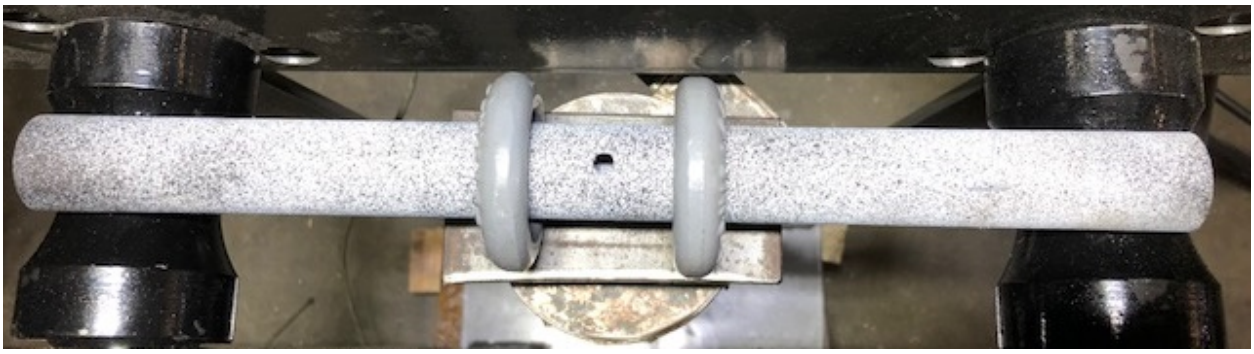

Exhibit 14: Physical test set-up of carbon fiber tube for DIC data collection.

Exhibit 15 shows a comparison of the z-direction (vertical) displacement of the composite tube for the DIC and FEA at 300 lbf applied total load (before the buckling failure occurred). Note that the DIC displacement has been referenced from the edge of the field of view while the FEA has been referenced to the fixed supports. This is why the DIC contour plot shows a displacement of 0 inches at the edge of the field of view while the FEA contour plot shows approximately -0.04 inches of displacement at the same point. The FEA shows less vertical displacement at the edges of the hole than did the DIC, and this deviation increases as the loads increase. Although the displacements/strains are expected to be symmetric about the center, the measured values exhibit greater variation about the symmetry plane. This behavior indicates that, during testing, the loading at the two fixture points was not perfectly equal as simulated by FEA. This is one cause for the difference between the FEA and DIC results. The FEA can be modified to misalign the center supports vertically to cause a displacement that better resembles the measured displacement. Comparing an x-y displacement plot along an axial line would be informative as far as the differences in loading. Comparing the axial displacement may be useful as well, but the strain data (of later exhibit) is more useful.

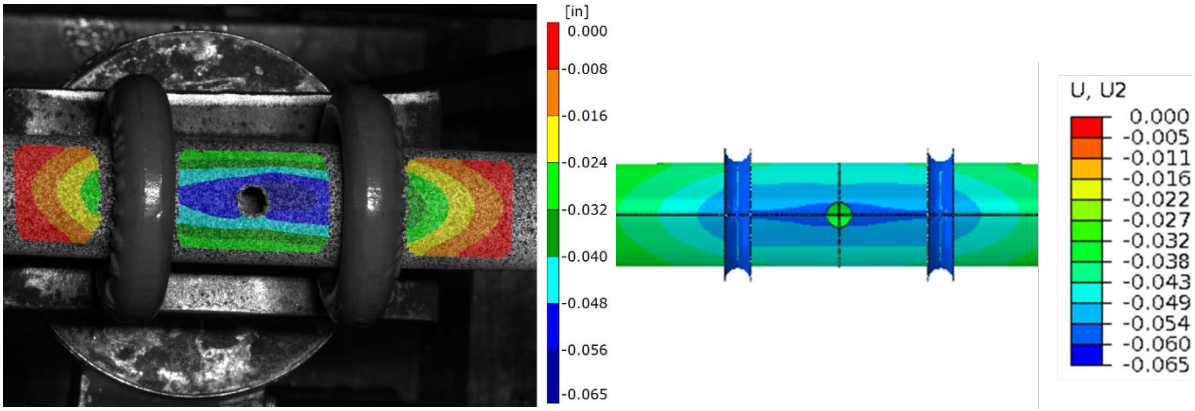

Exhibit 15: Contour plots comparing z-direction displacement between DIC (left) and FEA (right). Note that the two plots show different displacements at the edges of the fields of view shown

In Exhibit 16 and Exhibit 17, axial strain results are compared. Although the strain values measured during testing are different from the FEA results, the trends were similar in both cases. This discrepancy could have occurred due to several reasons (as discussed in the next section).

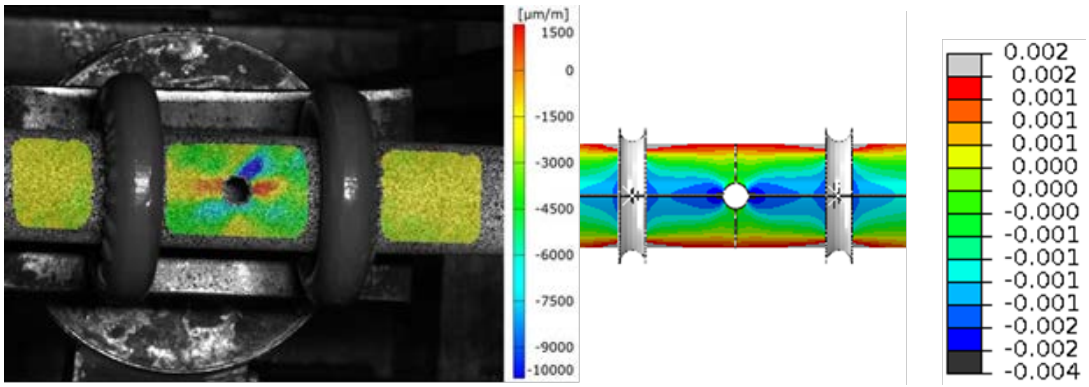

Exhibit 16: Contour plots comparing axial strain between DIC (left) and FEA (right).

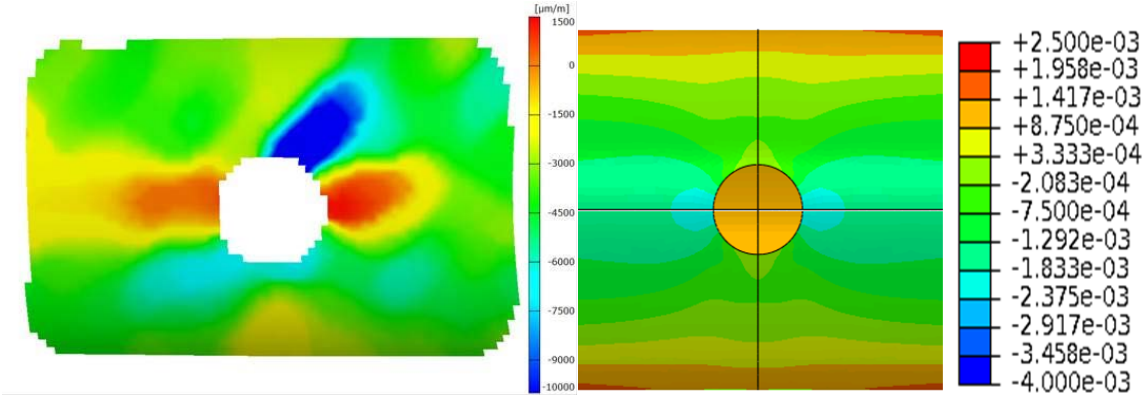

Exhibit 17: Comparison of DIC (left) and FEA (right) showing axial strains on composite tube at 300 lbf.

Although the FEA and DIC strain contour plots show the same general distribution, the magnitudes did not correlate well for a number of reasons. At higher loads, testing of the composite tube showed some damage near the hole, while the material model used in the simulation did not include any damage criteria. A linear elastic composite material model was used for the FEA, whereas the composite tube DIC results showed a nonlinear response at higher loads. The top ply in the composite tube (ply 5) is made of fibers woven together that run in 0° and 90° directions simultaneously; for modeling, this design was approximated by including two plies with half the thickness with fibers running in 0° and 90° as shown in Exhibit 12.

Additionally, the strain contours found using DIC indicate that the loading applied during the testing is biased between the two load application points, and that some twisting of the tube may have occurred. This can be seen in a plot of the axial strain along the center of the tube (Exhibit 18). This figure shows that the general shapes of the strain vs. location curves correlate and both increase with increasing applied load. However, the test data is not symmetrical about the hole due to a higher load being applied on one side. Exhibit 18 also shows a positive axial strain near the hole in the DIC results that does not appear in the FEA results. This outcome could be an effect of the woven outer ply vs. the half thickness ply approximation used in the FEM.

To fine-tune the model for better correlation, the difference in symmetric load can be adjusted as well as modifying the fiber orientation and properties (e.g., including nonlinear material response, a damage criterion etc.). The testing can be improved by using independent force applications so that each load can be controlled to match for a true four-point bend. The fixture alignment can also be improved to reduce any unintended side loading or twisting induced in the sample.

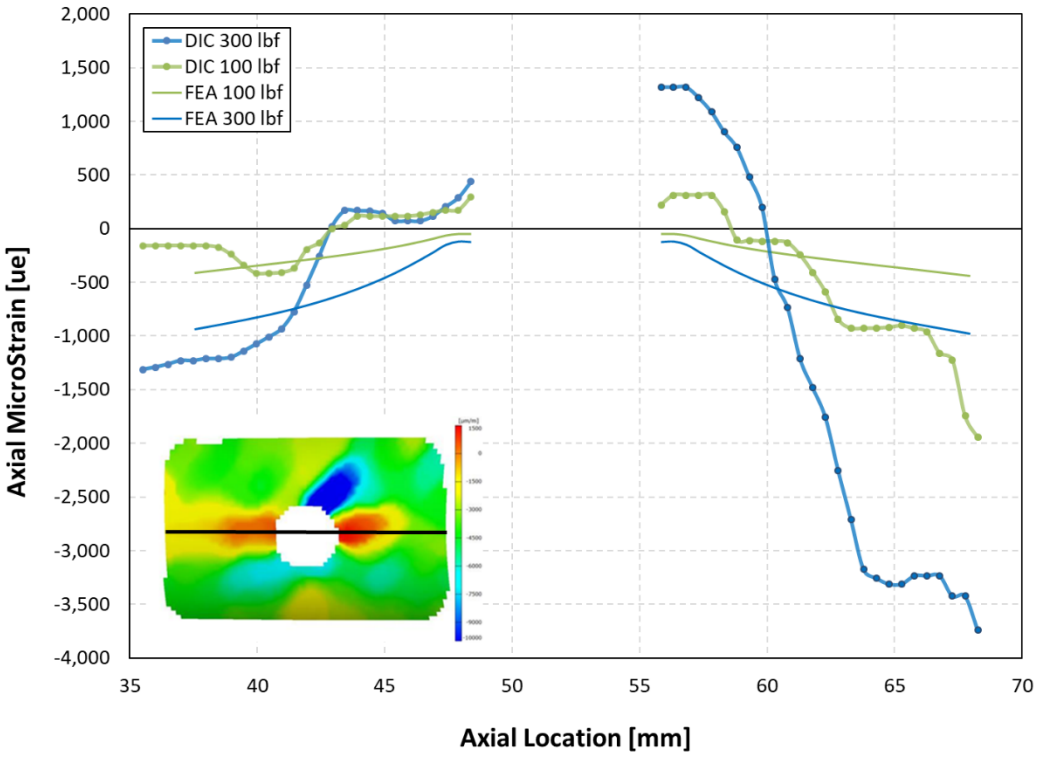

Exhibit 18: Comparison of DIC and FEA axial strain around hole.

After testing, the test article exhibited large fiber ruptures and delamination in the location and direction indicated by the maximum compression stresses in the DIC. This is shown in Exhibit 19. The failure seen here is typical for this type of loading and material.[17]

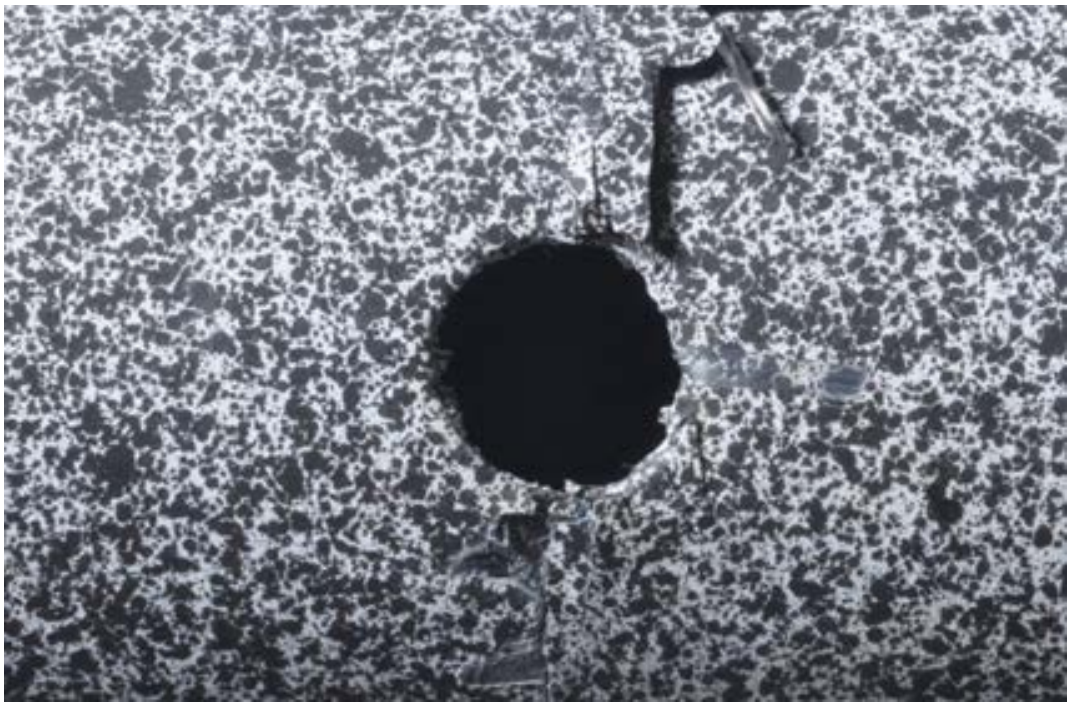

Exhibit 19: Photo of carbon-fiber composite tube after failure from local buckling (300 lbf of applied force).

Case Study 3: Compression of Additive Manufactured Complex Geometry Nozzle

To further investigate the correlation between DIC and FEA for more complex geometries, a 3-dimensionally complex geometry nozzle featuring converging and diverging concaves, rapid transitions, upsets, slots, and fillets was created. The design is shown in Exhibit 20. The objective was to represent some of the complex features that may be needed for parts in aerospace applications to meet challenging design constraints and complex loadings. The part features upper and lower flanges that can be loaded in compression via threaded fasteners on each side.

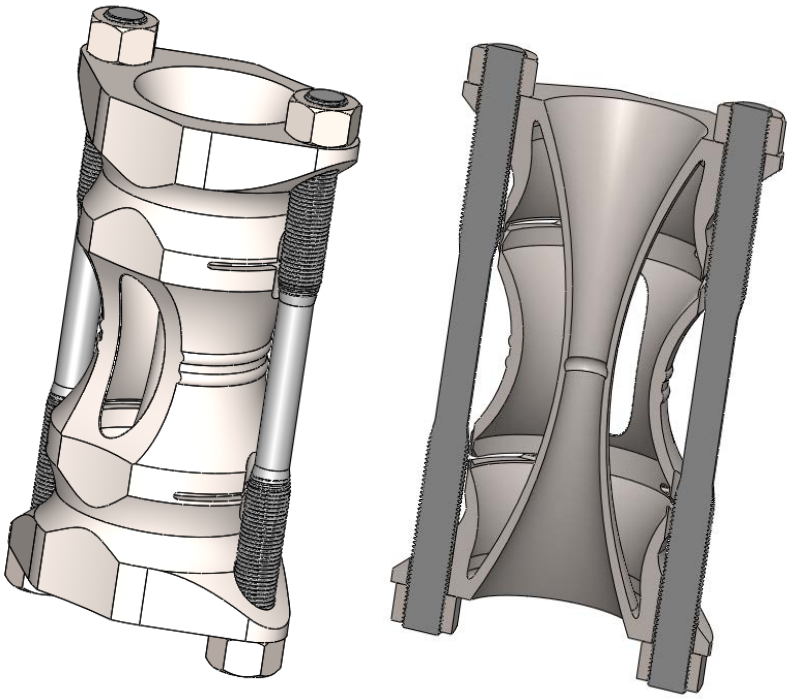

Exhibit 20: Parametric solid model representation of complex geometry nozzle.

FEA was first conducted on the model shown in Exhibit 21.

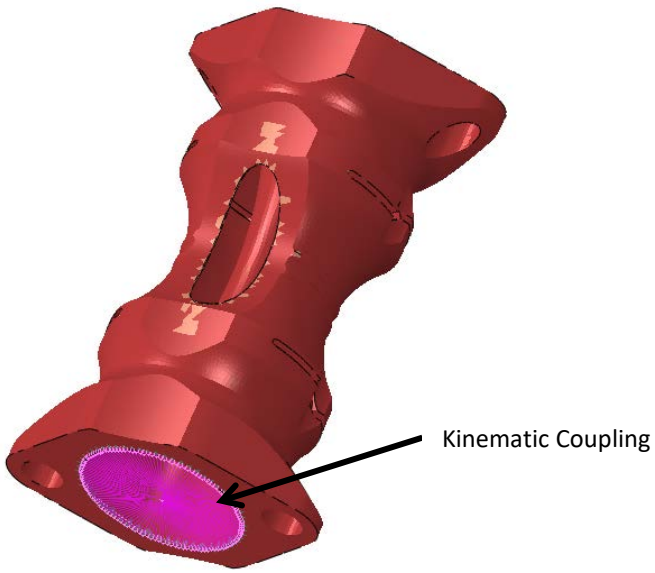

Exhibit 21: Finite Element Model for AM Nozzle

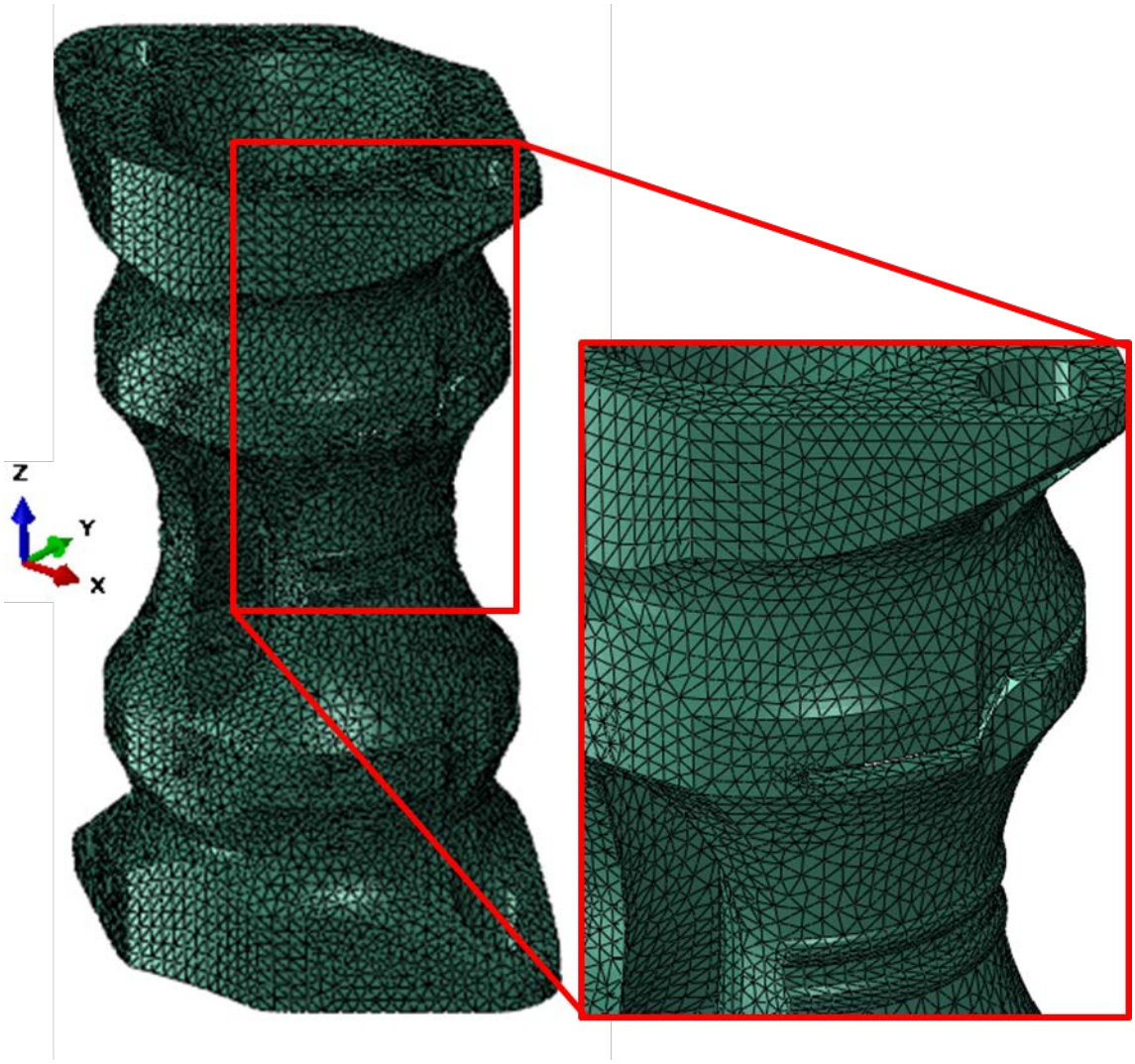

Exhibit 22: Finite Element mesh for AM Nozzle

The part geometry was built in Solid Works version 2017 and meshed in Abaqus using second-order tetrahedral elements (C3D10). The bolts in the FEA were modeled using beam elements (B31). A compressive load was applied by simulating loading from two bolts running axially in the outer flange holes. A pretension of 2,500 lbf was applied in each bolt. The material was assumed linear elastic with an elastic modulus of 29×10^6 psi in all directions. This is a FEM simplifying assumption used to highlight a difference in modeling versus real world material behavior. In the real world, the part's actual elastic modulus would be anisotropic in at least two directions—the vertical build direction and the horizontal direction. A static analysis was performed and large deformation theory was used. An Abaqus kinematic coupling definition was used to constrain the model and avoid any rigid body motion. As shown in Exhibit 21, a coupling was used in the FEM connecting the edge nodes to the center of the hole, which was fixed during the analysis. This coupling allows any radial displacement or ovalization of the connected nodes.

To obtain a physical representation of the 3D model used in the FEA, additive manufacturing was used to 3D print the part from Alloy 718. The part was made with the Powder Bed Laser Sintering (PBLS) technique in a Renishaw AM400 machine with 400-Watt laser power in 60-micron layers. The part was not heat-treated or Hot Isostatic Pressed (HIPed) prior to testing.

Sixteen rectangular rosette 350 Ohm foil resistance strain gages were installed in key areas on one-half of the nozzle for comparison to FEA. The gages had an effective gage length of 0.062”. The DIC speckle pattern was sprayed on the symmetrical half without strain gages (Exhibit 23).

Testing consisted of using two threaded rods and nuts to apply a compressive load across the part. Four strain gages were installed on each rod to measure the loads applied as the nuts were tightened. A standard elastic modulus of $30x10^6$ psi was used for the steel rods in order to calculate the corresponding stress and load from the average strains measured by the four strain gages on each rod. The DIC cameras were set up to capture the speckle pattern region.

Load was increased in stages by applying torque to the nuts, and DIC images were captured at each load stage for comparison to the initial (undeformed) state. Load was maintained as equal as possible between the two threaded rods at each load stage. Load in the two rods was able to be maintained within ±10 pounds.

A maximum final load of approximately 5,000 lbf was applied to the part (2,500 pounds applied by each threaded rod). DIC strains measured at this maximum load are shown in Exhibit 25. The nuts were then slowly loosened to relieve load on the part.

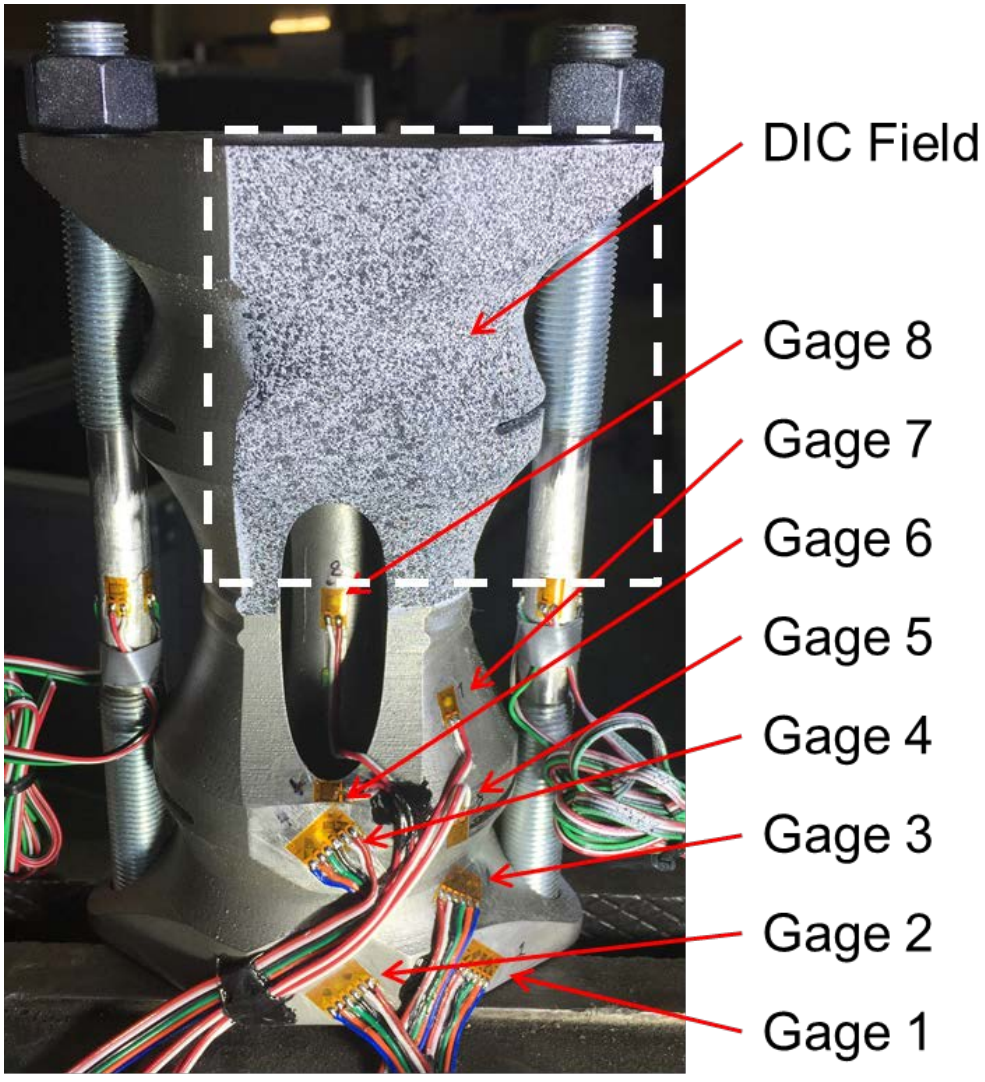

Exhibit 23: Photo of AM Nozzle test set-up

Plots of the load vs. strain for each of the foil strain gages is shown in Exhibit 24. The results follow a linear trend up to the maximum applied load. Note that the stain results correspond to the axial direction strain gage measurements except for Strain Gage 6, which was installed in the hoop direction.

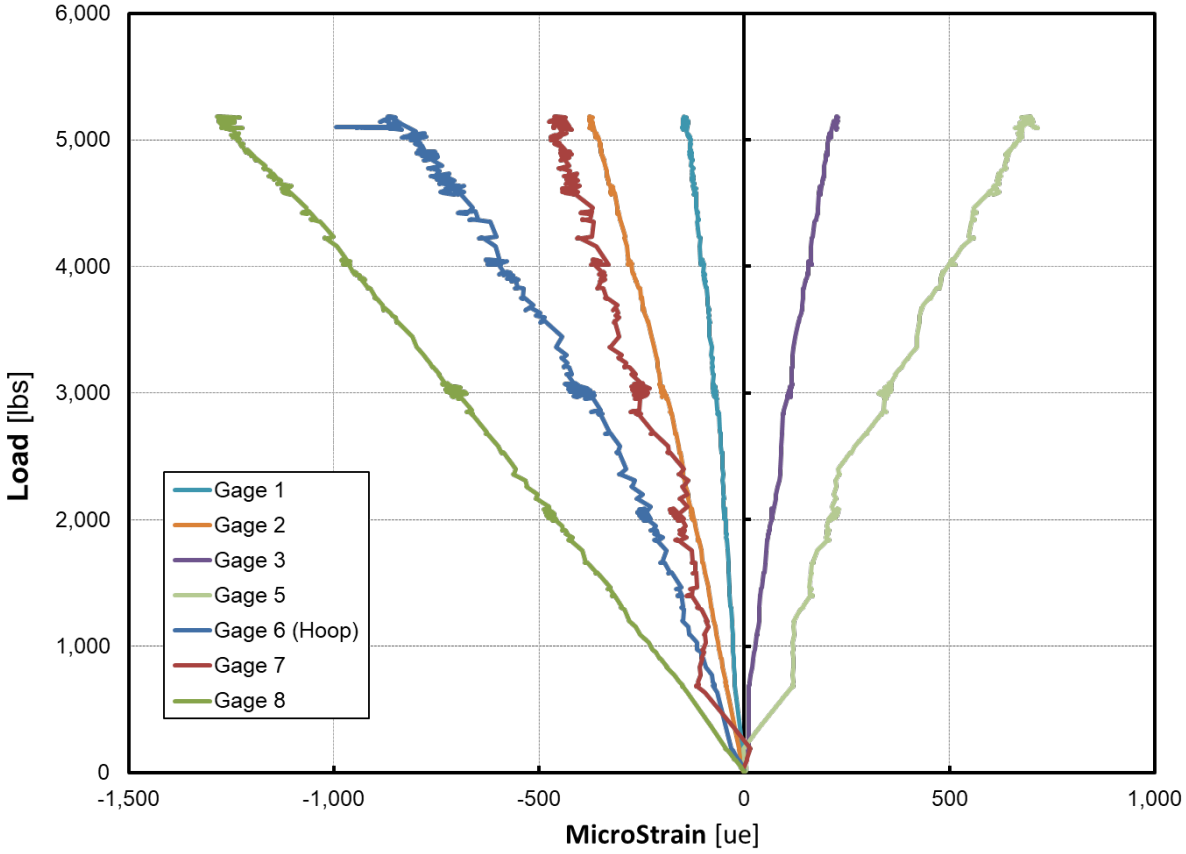

Exhibit 24: Strain gage data vs. load for AM Nozzle

Contour plots comparing results from DIC and FEA are shown in Exhibit 25. The plots show hoop strain and axial strain.

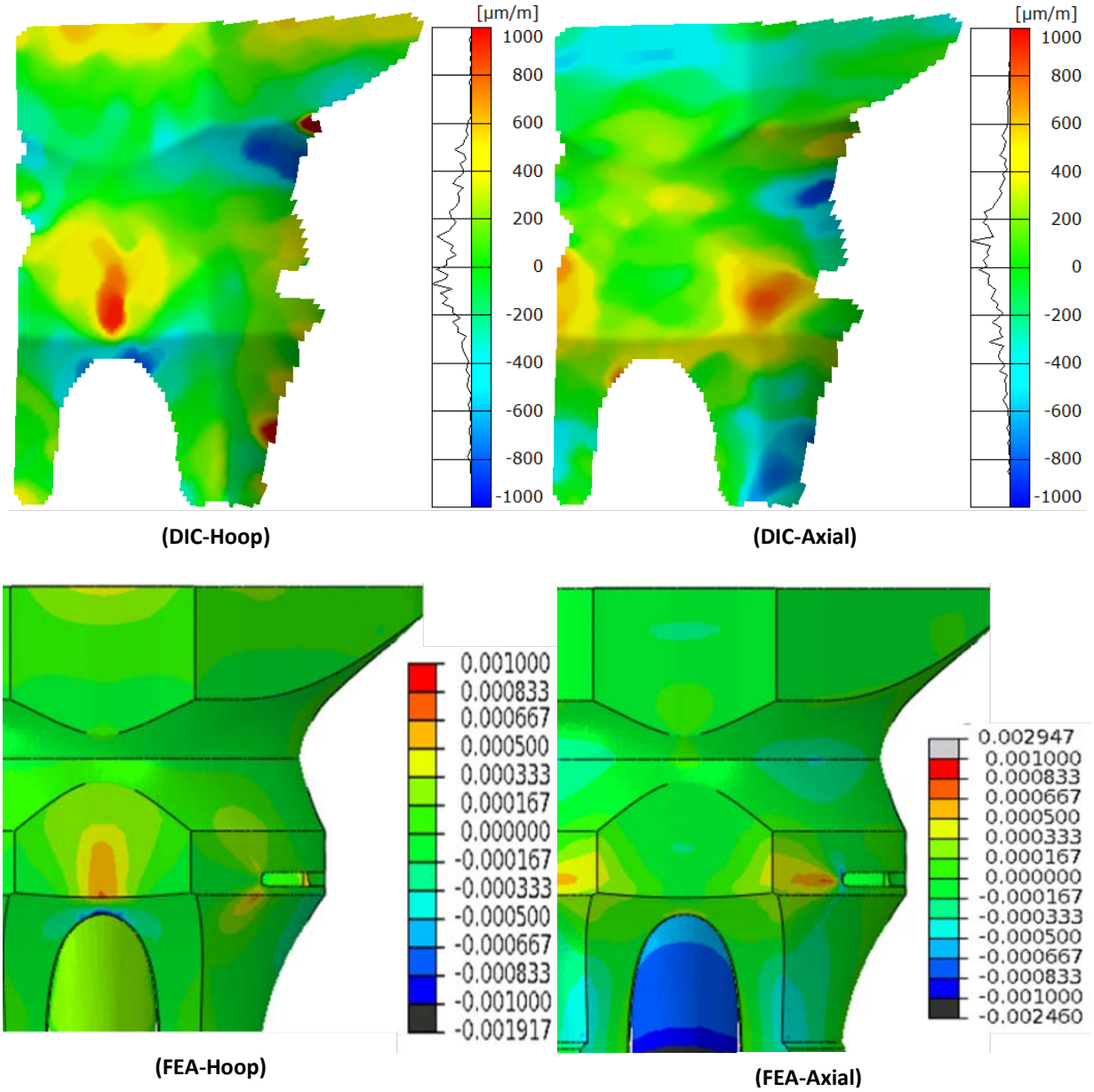

Exhibit 25: Comparison of AM Nozzle strains from DIC data (upper) and FEA (bottom) for hoop and axial strain.

Table 3: Comparison of Axial Microstrain for Strain Gages, FEA, and DIC at 5,000 lbf total load.

Measurement Device	Location 1	Location 2	Location 3	Location 4	Location 5	Location 6*	Location 7	Location 8
Strain Gage	150	-376	224	NA	714	-866	-465	-1,273
DIC	0 to 200	-500 to -300	0 to 500	-150 to 200	0 to 1,000	-900 to -400	-600 to -400	NA
FEA	0 to 167	0 to -500	-167 to 167	-167 to 167	0 to 1,000	0 to -833	-667 to -167	-2,460

*Note: For Strain Gage location 6, the uniaxial strain gage was placed in the hoop direction; therefore, hoop direction results are used for comparison.

Discussion of the Three Case Study Findings

In **Case Study 1**, DIC was found to be capable of enhancing FEA analysis by capturing data at strains beyond material yield and up to failure. For FEAs where post-yield behavior or failure conditions are of interest, DIC data provides a basis for analysis by enabling the creation of a damage model. Metallic materials are most often characterized using Material Test Reports (MTRs) generated via tensile testing of a round or flat test coupon. These MTRs normally provide the yield and ultimate tensile stresses of the material, as well as modulus of elasticity, elongation to failure, and reduction of cross-sectional area at failure in a single direction. For applications in which the material is expected to remain in the elastic region, these material properties, particularly yield stress and modulus of elasticity, are generally sufficient to predict the material behavior with an FEM. However, in applications in which the material may exceed the yield point and enter the plastic region, or for modeling the failure behavior of a structure, these measured properties are generally not adequate to perform an FEA with acceptable accuracy. DIC can be used to better characterize the material well beyond the elastic region, even to the point of material failure, providing additional data used in the development of a failure model in the FEM.

Material test labs performing tensile tests often use clip gages or other similar displacement measurement devices to measure the elongation of samples during testing. However, these types of gages are limited in their range of extension and are susceptible to shock damage if they are attached to the test sample during failure. These gages can only provide the elongation over the total length of the gage, which can be used to calculate the average strain over that length. This information is sufficient before necking of the specimen has occurred, when the strain remains constant over the gage length. However, once necking begins the engineering strain varies significantly along that length. Resistive strain gages can be applied to measure the strain at an exact location (subject to the size of the strain gage) and may or may not be able to be placed in the area of necking. If placed in the area of necking most strain gages would not have the ability to accurately measure elongation at such high strains.

DIC used during tensile testing provides data describing elongation of the gage length, as well as the full strain field along the sample, including after necking has occurred and all the way to failure. With DIC, strain along multiple directions can also be measured. The maximum displacement and strain limits for DIC are well beyond those of clip gages and resistive strain gages, and beyond the elongation and strain at failure for metals. This advantage applies to full-scale testing as well as the small-scale tensile testing discussed here.

Case Study 2 showed that local buckling in complex materials and geometries is difficult to predict or model on the first attempt. Composite materials often present a challenge in both modeling and comparing to real-world systems due to anisotropic behavior over small areas as well as high elongations. DIC can be used to capture the desired strain measurements for fine-tuning and validating FEMs of these materials. In this composite material case study, the test article eventually failed from local buckling, which was not initially captured in the FEA. The buckling may have occurred due to imperfections within the composite matrix or actual details of the geometry that the DIC was able to pick up but the FEA could not. Changes to the FEM that might improve its accuracy include adjusting the fibers and reassigning orientations and layers as well as modulus properties. With the full field of view and post-processing capabilities of DIC, local buckling can be measured and accounted for when comparing to FEM.

In **Case Study 3**, an anisotropic additive manufactured nozzle with a complex geometry showed relatively good agreement between the DIC test data and FEA in locations of peak strain locations and gradients. The peak strain magnitudes varied notably; this difference was most likely due to the elastic modulus used in the FEA. The FEA was assigned a constant 29×10^6 psi (200 GPa) modulus of elasticity in all directions; however, in the as-built condition the component could have had an anisotropic elastic modulus of near 29.4×10^6 psi (203 GPa) in the horizontal direction and 27.7×10^6 psi (191 GPa) in the vertical (build) direction.[18] These values could change as a result of post-manufacturing heat treatment or HIP processes. The DIC test data can be used to validate or improve the FEM.

Comparing the FEA and DIC data to strain-gage results demonstrated that it is difficult to exactly match strain gage test data. Strain gages have traditionally been used to help validate analytical models using testing results. Practically speaking, however, it is often difficult to achieve agreement between the strain gage data and the model (within 10% is challenging to achieve). One important reason for this is the physical placement of the gages in the stress field. In areas of high stress gradients, it is very difficult to accurately place a strain gage that precisely measures the strain at the desired location. Due to the design of a foil resistance strain gage, the gage can only measure an average strain in the surface onto which the gage is bonded. Therefore, there is a limit as to how small of an area can be measured precisely. In most cases, the areas of greatest interest have high strain gradients rather than constant stresses, and therefore strain gages are only placed in less interesting areas of low strain gradient in order to try to match the FEM.

With DIC (sometimes referred to as an optical strain gage), the area of strain measurement is limited only by the camera resolution and field of view. With today's high-resolution digital cameras, strain measurements over very small areas or areas of high strain gradients can readily be achieved. An example of this is seen in Table 3, where a strain range (strain gradient) is given by the DIC for the same area covered by a strain gage, which only provides a single (average) value. Another advantage of using a DIC system is that anything in the camera's field of view is captured during testing. With strain gages, locations must be selected prior to testing, with the possibility of discovering after the test that the gages were not attached at optimal locations. With DIC, a very large area can be speckled and recorded so that additional areas can be investigated efficiently after the initial analyses. With strain gages, the time, expense, and access limitations of the installation often limits the number of locations that can be evaluated.

When attempting to measure buckling for example, it is difficult to predict the buckling location before testing so that stain gages can be attached at/near that location. With DIC systems, an entire area can be recorded during testing. After the buckling or high strain occurs, the precise area of interest can then be focused on for comparison. With the increased evaluation options provided by DIC, comparisons of entire strain fields can be made to the FEA as opposed to only distinct individual points where strain gages were located. Strain gages also have limitations with respect to the range of data they can measure. For example, DIC systems can measure very high elongations (greater than 500,000 με), whereas strain gages (depending on the type) are often limited to 30,000 to 50,000 με. Strain gages are also limited by temperature, fatigue, and ability to bond to the surface. Since DIC does not contact the surface of the test article, it does not impose these limitations.

DIC does have limitations as wekk. Primary among these, DIC data can only be recorded in areas that can be seen by the cameras. The cameras need to be some distance away from the object of interest in order to get the proper field of view. Some space-limited situations may not allow for this. Strain gages can be completely out of sight, providing an important advantage in this regard such as measuring bolt pre-load or inside cavities. A combination of DIC and strain gage data with proper testing gives the best opportunity for comparison to an FEA.

Being able to gather more extensive strain measurement data allows for a more thorough comparison to FE models. DIC data can account for anisotropic material behavior as well as actual geometries. This in turn provides better possibilities for fine-tuning or calibrating FEM with empirical test data.

SUMMARY

The complex and structurally demanding aerospace designs of today call for increasingly complex Finite Element Models and Analyses. Since these models are mathematical approximations of real-world systems, there is a need to validate them with empirical testing. This approach is common by many aerospace agencies.[19] Digital Image Correlation can be used as a tool to enhance the FEA that is performed on complex geometries or anisotropic materials. DIC test data can enhance FEA by refining the assumptions used in the FEA model such as boundary conditions, material properties, and actual geometries. DIC offers the ability to account for such variables and make adjustments to the FEM. DIC offers notable advantages over foil strain gages: it is difficult to obtain a precise

measurement in high stress gradient areas using strain gages; strain gage results are limited to the number and location of gages installed; and strain gages are limited by factors such as high strains, high temperatures, and surface adhesion.

Three case studies were presented: (1) a uniaxial tension to failure test to consider the correlation beyond yielding and up to failure, (2) a carbon-fiber composite tube with a hole in four-point bending to compare buckling prediction and composite anisotropic materials, and (3) an additive manufactured part to investigate compression and bending results in very complex geometries in an additive material.

Differences were observed between the FEA and DIC results in these examples; difference between FEA and DIC can be attributed to one or a combination of the following reasons:

1. A linear elastic material model may be used for FEA while actual systems show nonlinear responses at higher loads. DIC can be used to better characterize a material well beyond the elastic region, even to the point of material failure. An FE damage model is helpful for applications in which some or all of the material may exceed the yield point and reach the plastic region, or for modeling the failure. FE simulations that do not include damage criteria can significantly diverge from real-world results when high loads and strains and damage occur. DIC test data can be used to create or validate a damage model within the FEM.
2. For composite structures, the fiber orientations, directions, and properties are difficult to model and are sometimes approximated in FEA. DIC test data can be used to account for these variables.
3. The assumed modulus of elasticity plays a large role in FEA and may not be properly accounted for. For composite or additive manufactured parts, the modulus is not constant through the structure. Additive manufactured part properties depend on many factors including build direction, energy input, build speed, chamber conditions, and others. DIC allows multidirectional properties from an actual test article to be used for input into FEMs.
4. Actual test article geometry can exert an influence on correlating FEM with real-world results and not all geometrical variations or tolerances are always considered. FEMs are typically based on nominal and perfect geometries, which do not exist in the real world. DIC data account for the actual geometries of test articles and can therefore show strains and stress more accurately.
5. Incorrect friction factors for models with composite or multiple parts can influence the FEA. DIC data can be used to help adjust these assumptions.
6. Real-world loading and testing conditions are never perfect. Symmetrical loading is often not perfectly balanced. Test fixtures can induce unaccounted for point loading, bending, or torsion that is not simulated in the FEM. Having DIC test data available can help make this apparent.

While FEA, Testing, and DIC all have limitations individually, a combination of good test methods, DIC data, strain gages, and a solid understanding of FEA will provide the best opportunity for gaining understanding of how complex materials and geometries perform under load to aid in the design process.

FUTURE WORK

Future work is needed to implement FEA model fine-tuning strategies described here with an iterative process of analyzing the test data with each updated model. Further testing can be performed to refine the applied loads for better correlation to the FE models. ASTM coupon tensile testing should be performed with additive manufactured material test coupons built alongside the AM nozzle. These efforts will increase the understanding of how to adjust the FE models for use with such materials. It would also be of interest to investigate a complex loading condition on the AM Nozzle such that the bolts are pre-tensioned and then the entire assembly is then loaded in compression. This will investigate the complex load distribution of pre-tensioned joints, which are common in real-world applications.

ACKNOWLEDGEMENTS

SES would like to thank James Hyder and Michael Corliss with Knust-Godwin for supplying the additive manufactured test article.

REFERENCES

[1] ASME, Guide for the Verification and Validation of Computational Solid Mechanics, American Society of Mechanical Engineers, ASME-V&V-10-2006, New York, 2006.

[2] Raju, Ivatury S., Knight Jr., Norman F., Shivakumar, and Kunigal N., "Some Observations On The Current Status of Performing Finite Element Analysis," NF1676L-19037, NASA Technical Reports Server, April 29, 2015.

[3] Thacker, Ben H., Doebling, Scott W., Hemez, Francois M., Anderson, Mark C., Pepin, Jason E., Rodriquez, Edward A., "Concepts of Model Verification and Validation," Los Alamos National Laboratory, LA-14167-MS.

[4] Flom, Yury, "Failure Assessment of Stainless Steel and Titanium Brazed Joints," GSFC.CP.5986.2012, NASA Technical Reports Server, May 21, 2012.

[5] Girolamo, Donato, and Dávila, and Carlos, G., "Adhesive Characterization and Progressive Damage Analysis of Bonded Composite Joints," NF1676L-18657, NASA Technical Reports Server, May 08, 2014.

[6] Luo, P., Chao, Y., Sutton, M., and Peters, W. 1993, "Accurate measurement of three-dimensional deformations in deformable and rigid bodies using computer vision," Exp Mech 33, 123–132.

[7] Lovejoy, Andrew E., Hilburger, Mark W., and Gardner, Nathaniel W., "Test and Analysis of Full-Scale 27.5-Foot-Diameter Stiffened Metallic Launce Vehicle Cylinders," AIAA SciTech Forum, Kissimmee, Florida, January 8-12, 2018.

[8] Telford, Robert, Peeters, Daniël, Oliveri, Vincenzo, Zucco, Giovanni, Jones, David, O'Higgins, Ronan, and Weaver, Paul M., "Enhanced Buckling Performance of a Stiffened, Variable Angle Tow Thermoplastic Composite Panel," AIAA SciTech Forum, Kissimmee, Florida, January 8-12, 2018.

[9] Moerman, K.M., Holt, C.A., Evans, S.L., and Simms, C.K., 2009, "Digital image correlation and finite element modelling as a method to determine mechanical properties of human soft tissue in vivo," J. Biomech., 42, pp. 1150–1153.

[10] Wang, W.; Roubier, N.; Peul, G.; Allain, J.M.; Infante, I.C.; Attal, J.P.; Vennat, E., "A new method combining finite element analysis and digital image correlation to assess macroscopic mechanical properties of dentin," Materials 2015, 8, 535–550.

[11] Rudd, Michelle T., Hilburger, Mark W., Lovejoy, Andrew E., Lindell, Michael C. and Gardner, Nathaniel W., "Buckling Response of a Large-Scale, Seamless, Orthogrid-stiffened Metallic Cylinder," AIAA SciTech Forum, Kissimmee, Florida, January 8-12, 2018.

[12] Lynn, Keith C., Dixon, Genevieve, "Flexural Fillet Geometry Optimization for Design of Force Transducers used in Aeronautics Testing," NF1676L-20232, NASA Technical Reports Server, April 29, 2015.

[13] Sutton, M.A., Orteu, J.-J., Schreier, H.W., 2009. Image correlation for shape, motion and deformation measurements: basic concepts, theory and applications. Springer, New York.

[14] Orteu, J.J., 2009. 3-D computer vision in experimental mechanics. Opt. Lasers Eng. 47, 282–291.

[15] GOM, 2013, *ARAMIS User Information – Hardware Sensor Configuration Examples*, GOM mbH, Braunschweig, Germany.

[16] ABAQUS, 2014, *ABAQUS Theory Manual and Analysis User's Manual* (Version 6.14), Dassault Systèmes Simulia Corp., Providence, RI, USA.

[17] Ambur, Damodat R., Jaunky, Navin, Davila, Carlos G. and Hilburger, Mark, "Progressive Failure Studies of Composite Panels with and without Cutouts," AIAA Paper 2001-1182, NASA Technical Rpt Server, August 17, 2001.

[18] Renishaw Material Data Sheet, H-5800-1052-03-A_In718-0405, July, 2017

[19] NASA Technical Standard NASA-STD-7009A, "Standard for Models and Simulations," July 13, 2016.